Journal of Physics and Chemistry of Solids 75 (2014) 8–14

Contents lists available at ScienceDirect

Journal of Physics and Chemistry of Solids

journal homepage: www.elsevier.com/locate/jpcs

The luminescence and structural characteristics of Eu^{3+}- doped $NaSrB_5O_9$ phosphor

G.R. Dillip [a], K. Mallikarjuna [a], S.J. Dhoble [b], B. Deva Prasad Raju [c,a,*]

[a] Department of Physics, Sri Venkateswara University, Tirupati – 517 502, India
[b] Department of Physics, RTM Nagpur University, Nagpur – 440 033, India
[c] Department of Future Studies, Sri Venkateswara University, Tirupati – 517 502, India

ARTICLE INFO

Article history:
Received 2 March 2013
Received in revised form
22 June 2013
Accepted 8 July 2013
Available online 31 July 2013

Keywords:
A. Inorganic compounds
B. Chemical synthesis
C. Infrared spectroscopy
D. Microstructure
E. Luminescence

ABSTRACT

A red-emitting phosphor $NaSrB_5O_9:Eu^{3+}$ was synthesized by employing a solid-state reaction (SSR) method. The structures of the phosphors were analyzed by X-ray diffraction (XRD), Fourier-transform infrared (FTIR) and Raman studies. The band at ~282 nm in the excitation spectra indicated the charge transfer band (CTB) of B-O in the host, whereas the CTB of Eu-O was observed at ~275 nm for the $NaSrB_5O_9:Eu^{3+}$ (Eu^{3+} = 1 at.%) phosphor, which was supported by diffuse reflectance spectroscopy (DRS) measurements. The photoluminescence (PL) measurements exhibited a strong red emission band centered at about 616 nm ($^5D_0 \rightarrow {}^7F_2$) under an excitation wavelength of 394 nm ($^7F_0 \rightarrow {}^5L_6$). Upon host excitation at 282 nm, the pristine $NaSrB_5O_9$ exhibited a broad UV emission centered at ~362 nm. The energy transfer from host to Eu^{3+} ions was confirmed from luminescence spectra, excited with a 355 nm Nd:YAG laser. In addition, the asymmetric ratios indicate a higher local symmetry around the Eu^{3+} ion in the host. The calculated CIE (Commission International de l'Eclairage) coordinates displayed excellent color purity efficiencies (around 99.7%) compared to other luminescent materials.

1. Introduction

White light emitting diodes (W-LEDs) have been investigated as a next generation solid-state lighting sources to supplant conventional light sources, such as incandescent lamps, fluorescent lamps and high pressure sodium vapour lamps. These devices can potentially help alleviate various ongoing problems, like energy crises and environmental pollution [1,2]. The demand for W-LEDs has grown enormously in various fields, such as in large size flat panel backlighting, street lights, vehicle forward lamps, and museum illumination, because of their advantages over traditional light sources. Such advantages include their relatively cool operating temperature, higher energy efficiency, brightness, low volume, long persistence, low power consumption and environment-friendliness [3,4]. Currently, inorganic luminescent materials (also known as phosphors) are being used in phosphor-converted W-LEDs, due to their low-costs, compact sizes and required colors. For W-LED applications, a new crystal structure class of inorganic borate-based materials has been receiving a great deal of attention [5]. It is well known that boron can coordinate with oxygen to form a variety of atomic groups, which are considered to be a dominant factor for determining the physical and optical properties of borates. Moreover, anionic radicals in the borate class can acquire B-tetrahedral or/and B-triangles, and these groups may be further linked via common oxygen atoms to form isolated rings and cages or polymerize into infinite chains, layers and networks, leading to the rich structural chemistry [6]. As far as luminescence is concerned, much attention has been contributed to alkali alkaline-earth metal borate lattices doped with rare-earth (RE) ions, because they have high luminescence, moderate synthesis temperatures, high color purities and low thermal degradation. As conversion phosphors for white-light LEDs, these materials must have high absorption in the near-UV to blue spectral region (370 – 470 nm), high quantum efficiency (≥ 90%), high thermal and chemical stability, low thermal quenching and maintenance of high quantum efficiency in an encapsulating polymer matrix as well as minimized degradation. Unfortunately, there are very few existing phosphor materials that can efficiently convert UV-blue emissions from LEDs into green, and in particular, red light. In addition, red-emitting phosphors that can be efficiently pumped by UV-blue LEDs are very scarce. With respect to the current applied phosphors for W-LEDs, $YAG:Ce^{3+}$-based phosphors exhibit poor color rendering indexes (CRI ≈ 70-80), reduced efficiency caused by thermal quenching and they suffer from reduced lifetimes because they lack red components [7,8]. Therefore, alternative phosphors with improved properties are in demand and they urgently need to be prepared, characterized and

* Corresponding author at:. Sri Venkateswara University, Department of Future Studies, Tirupati 517 502, India. Tel.: +91 94402 81769.
E-mail address: drdevaprasadraju@gmail.com (B.D.P. Raju).

0022-3697/$ - see front matter © 2013 Elsevier Ltd. All rights reserved.
http://dx.doi.org/10.1016/j.jpcs.2013.07.008

tested under application conditions. Among the various RE elements, the Eu^{3+} ion is an important trivalent RE ion that has been applied in borates, phosphates, oxides, vanadates, molybdanates, and in other materials for red emission because of its chemical and thermal stability.

In the past, RE ion-doped borates have been utilized in luminescence materials, for instance, in BaB_2O_4:Eu^{3+} [9], $Al_3GdB_4O_{12}$:Eu [10], $LuAl_3(BO_3)_4$:Ce^{3+} [11], $Ca_3Y(GaO)_3(BO_3)_4$:Ce^{3+},Mn^{2+},Tb^{3+} [12], SrB_2O_4:Eu^{3+} [13], (Y,Gd)BO_3:Eu^{3+},Tb^{3+} [14], $NaSrBO_3$:Ce^{3+} [15] and $Ba_2Tb(BO_3)_2Cl$:Eu [16]. Keeping the above advantages in mind, we chose $NaSrB_5O_9$ as a host matrix and the Eu^{3+} ion as the dopant for our work. To the best of our knowledge, nothing has been published on the luminescence properties of Eu^{3+}-doped $NaSrB_5O_9$ phosphors. In this paper, we report our recent investigation results on the photoluminescence characteristics of red-emitting borate phosphor $NaSrB_5O_9$:Eu^{3+} and its application in W-LEDs pumped by near-UV light. In addition, structural, morphological and thermal studies were also performed and discussed.

2. Material synthesis

Polycrystalline samples of $NaSrB_5O_9$:Eu^{3+} were synthesized via a conventional SSR method, because the method is simple, cost-effective and convenient and it involves only a few solvents. For this, analytical grade Na_2CO_3, $SrCO_3$, H_3BO_3 and Eu_2O_3 were used as received without further purification. The nominal impurity (Eu^{3+}) content was varied from 0 to 9 at.% in the host matrix. First, stoichiometric amounts of the starting materials were mixed homogeneously in an agate mortar for 1 h. Later, each of the samples were put into porcelain crucibles and gradually heated to 800 °C in an electric furnace and kept at this temperature for 8 h. After sintering, the products were cooled down to room temperature (RT) inside the furnace itself and ground again into fine powder for further measurements.

2.1. Characterization

The phase purity of the reaction products were analyzed on a Rigaku Smartlab X-ray diffractometer with *Cu* K_α radiation (λ=1.5406 Å) at 40 kV and 20 mA. The data was collected over a 2θ range from 10–80° in the step scan mode with a step size of 0.02°. FTIR spectra were recorded on a Bruker Alpha-T FT-IR spectrophotometer using KBr pellets in the spectral range of 4000–500 cm^{-1}. Raman spectrum of $NaSrB_5O_9$:Eu^{3+} phosphor was recorded between 4000 and 200 cm^{-1}. The morphology of the sample was inspected using a field emission scanning electron microscope (FE-SEM, ZEISS, Japan). The elemental analysis was carried out by energy dispersive X-ray spectroscopy (EDS) on an FE-SEM-attached EDS instrument. Thermogravimetric analysis (TGA) and differential thermal analysis (DTA) was performed on an EXSTAR 6000 thermal analyzer at a heating rate of 10 °C/min and the temperature range was varied from RT to 700 °C. UV-Vis DRS was measured on a UV-Vis spectrophotometer (Jasco, Japan) using $BaSO_4$ as a standard measurement. PL spectra were recorded using a fluorescent spectrophotometer (Jobin Vyon Fluorolog–3) with a xenon lamp as an excitation source. All the measurements were performed at RT.

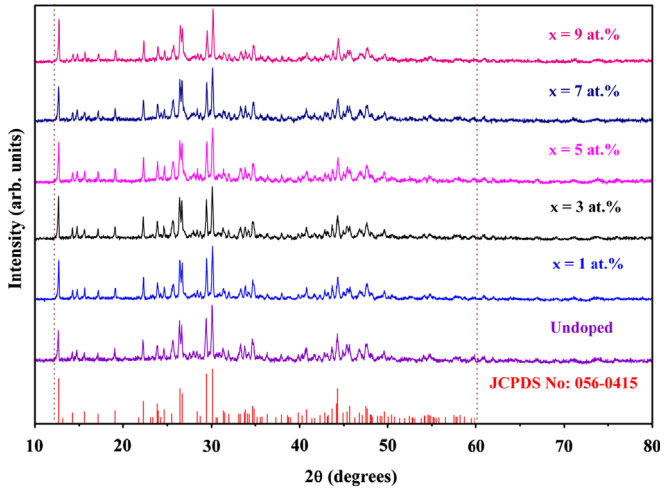

Fig. 1. XRD patterns of $NaSr_{1-x}B_5O_9$:Eu_x^{3+} (x =0 – 9 at.%) phosphors.

3. Results and discussion

3.1. XRD analysis

Fig. 1 shows the comparison of powder XRD patterns of $NaSrB_5O_9$:Eu^{3+} (Eu^{3+}=0, 1, 3, 5, 7 and 9 at.%) phosphors. The XRD peaks of the powders were found to agree well with those reported by JCPDS Card No. 56-0415, suggesting that the doped Eu^{3+} ions did not induce significant changes in the host structure. The absence of impurity phases indicated that the phosphor samples were well synthesized by the SSR method. These results indicate that the $NaSrB_5O_9$:Eu^{3+} phosphor has a relatively low sintering temperature, which is also consistent with the key requirement of energy saving for products in today's society. In 2007, *Wu et al.*,[17] reported the crystal structure of novel borate $NaSrB_5O_9$ by refining the powder diffraction pattern, which revealed a monoclinic crystal structure with space group $P2_1/c$ and the cell parameters were a=6.4963 (1) Å, b=13.9703 (2) Å, c=8.0515 (1) Å, β=106.900 (1)° and Volume=699.16 (2) $Å^3$. According to *Wu et al.*,[17] the fundamental structural unit in $NaSrB_5O_9$ is a $[B_5O_9]^{3-}$ group that is composed of three BO_3 triangles (Δ) and two BO_4 tetrahedrons (□) and the Sr atoms are surrounded by eight O atoms, forming trigonal dodecahedra. This kind of surrounding environment offers possibilities to stabilize a RE ion, when the position of Sr^{2+} is replaced by Eu^{3+} ions. Thus, the RE ion-doped borates will achieve various emissions, which can be correlated to the environment of the O atoms in the hosts. The ionic radii for eight-coordinated Sr^{2+} and Eu^{3+} are 0.126 nm and 0.107 nm, respectively [7]. On the basis of similar ionic radii between these two ions, we predicted that the possible sites for incorporating the Eu^{3+} ions is at Sr^{2+} sites of $NaSrB_5O_9$. Due to the difference in ionic radii between the two ions, the maximum intensity diffraction peak of the pristine $NaSrB_5O_9$ at 30.04° was shifted towards higher angles when the Eu^{3+} ion concentration was increased. Hence, the authors believed that the charge loss was most likely compensated by the Sr^{2+} vacancies (V_{Sr}) followed by $3Sr^{2+} \rightarrow 2Eu^{3+} + V_{Sr}$.

3.2. FTIR studies

In order to confirm the coordination surrounding the B-O in $NaSrB_5O_9$:Eu^{3+} samples, the FTIR spectra were recorded and are shown in Fig. 2. From the spectra, it is clear that the strong band at about 1316 cm^{-1} for all samples should be ascribed to the stretching modes of trigonally coordinated boron (BO_3) groups, while the bands near 1002 and 972 cm^{-1} mainly attributed to asymmetric stretching vibrations of tetrahedral boron (BO_4) groups. The bands associated with BO_3 and BO_4 out of plane bending modes overlap and are located in the range between 704 and 830 cm^{-1} [6]. Further, this confirms the existence of both trigonally and tetrahedrally coordinated boron atoms and these

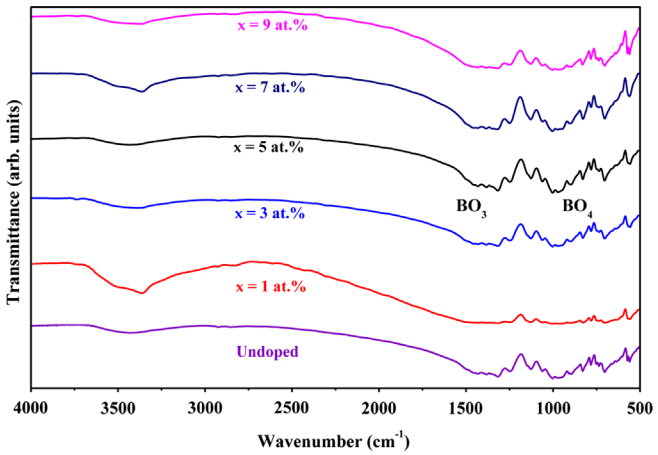

Fig. 2. FTIR spectra of $NaSr_{1-x}B_5O_9:Eu_x^{3+}$ ($x = 0 - 9$ at.%) phosphors.

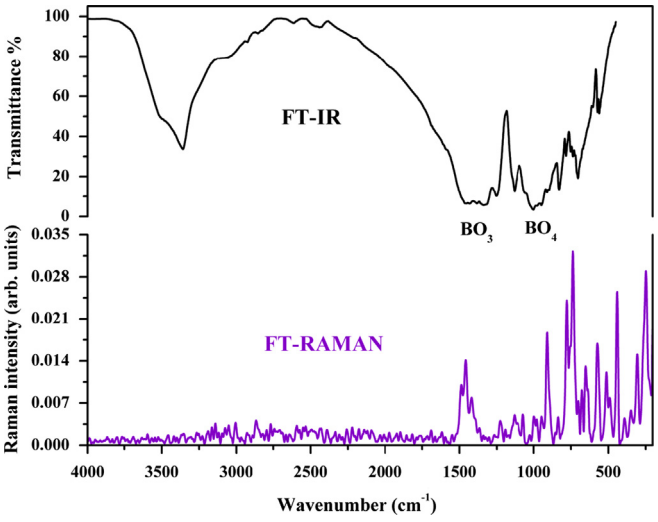

Fig. 3. Comparison of FT-IR and FT-Raman spectra of 9 at.% Eu^{3+}-doped $NaSrB_5O_9:Eu^{3+}$ phosphor.

values agree well with those reported in the literature for borates [18], and the results from the XRD analysis are also consistent with the results obtained by *Wu et al.*,[17]. The broad absorption band located at about 3430 cm^{-1} clearly indicated the presence of an -OH group in the samples, which is the characteristic vibration of water in air that has physically absorbed on the sample surface [19]. It is well known that the presence of -OH increases the optical losses and then decreases the quantum efficiency of RE ion-doped materials. However, in the present phosphors, the intensity of the IR band associated with the -OH group is extremely low, which indicates that the studied phosphors are suitable for practical applications.

3.3. Raman analysis

To further confirm the presence of trigonally coordinated boron (BO_3) and tetrahedral boron (BO_4) groups in the structure of the $NaSrB_5O_9:Eu^{3+}$ phosphor, the Raman spectrum of $NaSrB_5O_9:Eu^{3+}$ ($Eu^{3+}=9$ at.%) was also recorded and the comparative vibrational frequencies between IR and Raman studies are shown in Fig. 3. It can be seen from the spectra that the vibrational frequencies of the Raman spectrum match well with those of the IR spectrum, but the assignment of vibrations below 500 cm^{-1} is also observed in the Raman analysis. Literature overviews on the Raman measurements of borates with wavenumbers under 650 cm^{-1} in Raman spectra indicate that these peaks can be attributed to lattice and RE-O modes [20]. The characteristic features seen between 650 and 750 cm^{-1} and between 1350 and 1490 cm^{-1} correspond to triangular symmetric stretching and triangular asymmetric deformation of the BO_3 structure, respectively. The bands between 344 and 504 cm^{-1} and those between 1024 and 1156 cm^{-1} correspond to asymmetric stretching and tetrahedral distortion of BO_4, respectively [21]. The results of both IR and Raman spectra of the prepared powder confirmed that the boron atoms are trigonally and tetrahedrally coordinated to form the BO_3 and BO_4 groups in $NaSrB_5O_9:Eu^{3+}$, respectively.

3.4. FE-SEM and EDS analysis

FE-SEM has been used as powerful tool to vividly illustrate the sizes and morphologies of samples. An FE-SEM image of the $NaSrB_5O_9:Eu^{3+}$ ($Eu^{3+}=9$ at.%) phosphor is shown in Fig. 4(a). Generally, the size and morphologies of the particles depend on the various synthesis methods. In our present investigation, we used a one-step SSR method to synthesize the phosphors. With this method, the size of the particles mainly depends on the uniformity of grinding and homogeneity of the sample. From the figure, it is clearly observed that the microstructure of the phosphor is composed of irregular grains formed by aggregation. A detailed examination of the enlarged FE-SEM micrograph from a selected region (Fig. 4(b)) indicated that the average sizes of the particles are in sub-micrometer dimension and the surface of the irregular grains made up of the accumulation of more rods-like structure is seen in microgram [22]. To further investigate the presence of the europium element in the $NaSrB_5O_9:Eu^{3+}$ phosphor, an EDS analysis was carried out. A representative EDS spectrum of $NaSrB_5O_9:Eu^{3+}$ ($Eu^{3+}=9$ at.%) is depicted in Fig. 4 (c) and it confirmed the presence of the dopant (Eu) in the $NaSrB_5O_9:Eu^{3+}$ phosphor. In addition, the specific Au lines in the EDS spectrum show the presence of gold in the $NaSrB_5O_9:Eu^{3+}$ phosphor, which is due to the fact that a gold layer was coated onto the sample surface for conduction.

3.5. TGA/DTA studies

To elucidate the thermal properties of the $NaSrB_5O_9:Eu^{3+}$ phosphor, a TGA/DTA analysis was carried out. The results obtained from TGA and DTA studies for the $NaSrB_5O_9:Eu^{3+}$ ($Eu^{3+}=9$ at.%) phosphor are shown in Fig. 4(d). Based on the thermogram, there is no detectable mass loss in the prepared products between RT and 700 °C. However, the slight mass loss in the RT-150 °C range is ascribed from desorption of the absorbed water, which is consistent with FTIR results. The DTA shows an obvious exothermic broad band peaking at around 320 °C, which may be due to the evaporation of absorbed moisture present on the surface of the sample [23]. Further, no significant peaks were observed, which indicates the thermal stability of the sample prepared by the SSR method.

3.6. DRS analysis

The measured DRS of the $NaSrB_5O_9:Eu^{3+}$ ($Eu^{3+}=0$, 1, 3, 5, 7 and 9 at.%) phosphor are shown in Fig. 5. The image shows strong absorption bands at ~240 and 284 nm for the undoped $NaSrB_5O_9$ sample, which are due to boron to oxygen charge transitions (CT) in the $NaSrB_5O_9$ phosphor, which are consistent with the absorption bands obtained from excitation spectra [24]. When the Eu^{3+} ions were introduced into the host matrix, the band at ~240 nm shifted towards the higher wavelength region

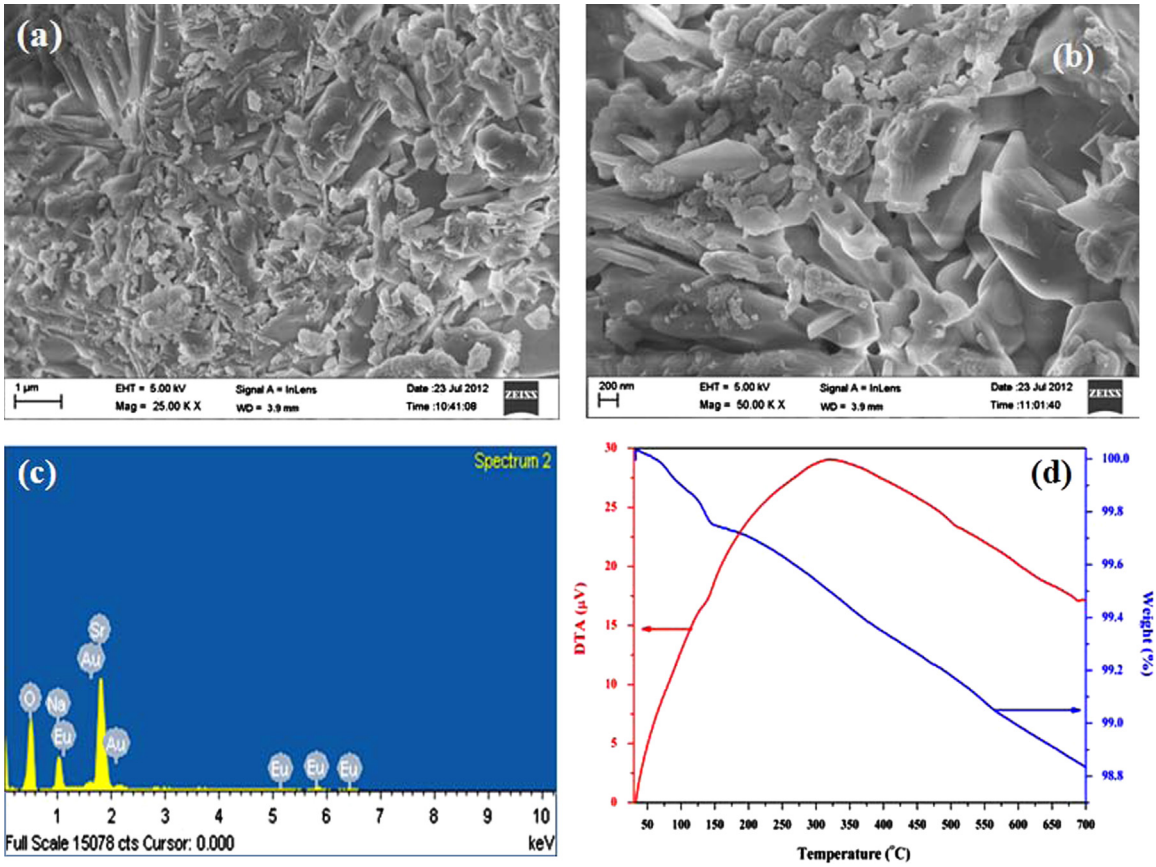

Fig. 4. (a) Low-magnification, (b) High magnification FE-SEM images, (c) EDS profile and (d) TGA/DTA trace of $NaSrB_5O_9:Eu^{3+}$ (Eu^{3+} = 9 at.%) phosphor.

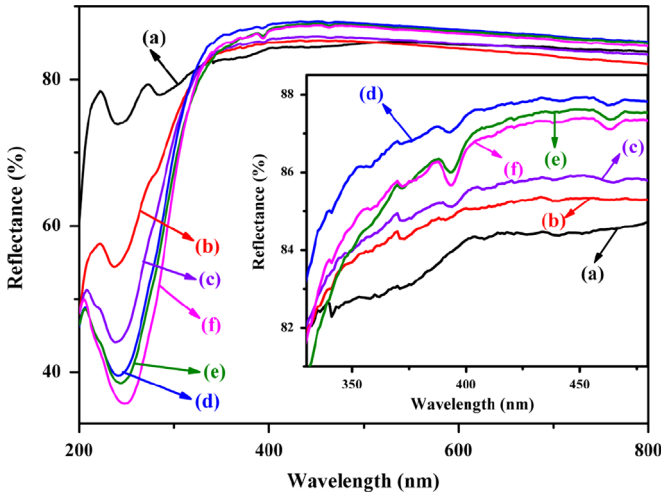

Fig. 5. UV-Vis diffuse reflectance spectra of $NaSr_{1-x}B_5O_9:Eu_x^{3+}$ (x = a - e = 0 – 9 at.%) phosphors. Inset shows the expansion of DRS from 330 to 480 nm.

between 240 and 250 nm due to the increasing Eu^{3+} ion concentration, while the band at ~284 nm disappeared, indicating the possible energy transfer from borate groups to Eu^{3+} ions in the $NaSrB_5O_9:Eu^{3+}$ phosphors. In addition, the DRS graph shows several absorption bands in the wavelength range from 330 to 480 nm (shown in the inset of Fig. 5), which is likely originating from the *4f* – *4f* transition of the Eu^{3+} ions. These bands are assigned to $^7F_0 \rightarrow {}^5L_7$ (~371 nm), $^7F_0 \rightarrow {}^5L_6$ (~394 nm), $^7F_0 \rightarrow {}^5D_3$ (~421 nm), and $^7F_0 \rightarrow {}^5D_2$ (~463 nm) [25]. From the DRS results, it was concluded that the Eu^{3+} ion-doped $NaSrB_5O_9$ host enhances the optical absorption in the near-UV region. Notably, $NaSrB_5O_9$ has a high optical absorption behavior, which means that these phosphors can be phosphor-converted materials for use in W-LEDs. Careful examination of DRS indicates that the intensity of the absorption bands increased as the Eu^{3+} ion concentration increased, which indicates the dopant ions were incorporated into the host lattices. The band at around 394 nm had the highest absorption, which is consistent with those observed in excitation spectra.

3.7. PL studies

The excitation spectra of the $NaSrB_5O_9:Eu^{3+}$ (Eu^{3+} = 0, 1, 3, 5, 7 and 9 at.%) phosphor that monitored the Eu^{3+} emission of the $^5D_0 \rightarrow {}^7F_2$ transition at 616 nm are shown in Fig. 6. For undoped sample in the range from 220-295 nm, the spectra consist of only one broad absorption band that peaks at ~282 nm, which is due to the charge transfer from B to O atoms in the $NaSrB_5O_9$ host [24]. It is also observed from the figure that when the Eu^{3+} ions are introduced into the $NaSrB_5O_9$ host, the spectra are comprised of two regions: One is a broad absorption band from 220–295 nm, another is several intense lines between 350 and 550 nm. The broad absorption band is assigned to the CTB of Eu - O [26], which occurs by electronic transition from the filled *2p* orbital of O^{2-} to the partially filled *4f* orbital of Eu^{3+}. The CTB is related closely to the covalency between O^{2-} and Eu^{3+} and the coordination environment around Eu^{3+} [27]. As the Eu^{3+} ion concentration increases, the CTB of Eu-O also increases and is shifted towards the shorter wavelength (*higher energy*) region. Variation of CTB with different Eu^{3+} ion concentrations is listed in Table 1. In order to understand the shifting of Eu-O CTB, the optical electronegativity of the ligand ion is calculated by using the Jorgensen empirical formula of charge transfer [28], which is expressed as

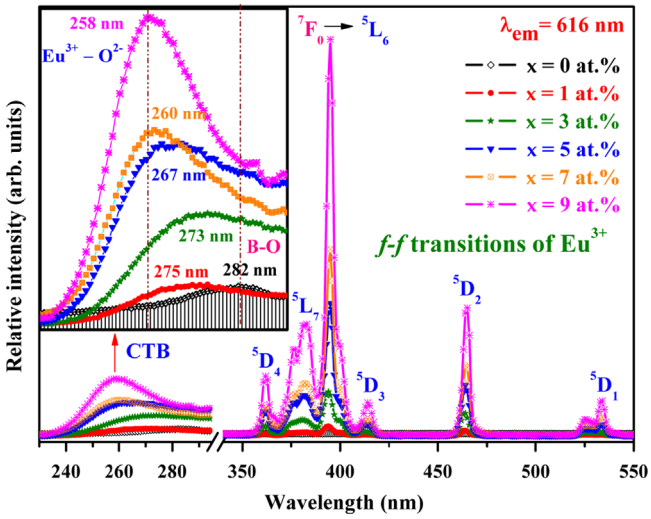

Fig. 6. Excitation spectra of $NaSr_{1-x}B_5O_9:Eu_x^{3+}$ ($x=0-9$ at.%) phosphors. Inset shows the expansion of CTB from 220-290 nm.

Table 1
Variation of CTB, difference in electronegativity, asymmetric ratio and color purity with the Eu^{3+} ions content in $NaSrB_5O_9$ phosphors.

Nominal Eu^{3+} content in host (at.%)	CTB (~nm)	Difference in Electronegativity $\sim\left(\chi\left(O^{2-}\right)-\chi\left(Eu^{3+}\right)\right)$	Asymmetric ratio (~R)	Color purity (%)
0	282	–	–	–
1	275	1.213	2.48	99.60
3	273	1.219	2.66	99.72
5	267	1.250	2.70	99.71
7	260	1.282	2.73	99.34
9	258	1.290	2.71	99.73

$\Delta_{Eu-O}=[\chi(ligand)-\chi(Eu^{3+}ion)]3\times10^4\,cm^{-1}$ where Δ_{Eu-O} is the peak position of the Eu-O CTB and $\chi(ligand)$ and $\chi(Eu^{3+}ion)$ are the optical electronegativities of the ligand ion (O^{2-}) and the Eu^{3+} ions, respectively [29]. It is well known that the optical electronegativity of the ion changes in different crystal field environments. From Fig. 6, the peak position values (Δ_{Eu-O}) of the Eu-O CTB are 274.8 nm (36390 cm^{-1}), 273.4 nm (36576 cm^{-1}), 266.6 nm (37509 cm^{-1}), 260.1 nm (38446 cm^{-1}) and 258.4 nm (38699 cm^{-1}) for $Eu^{3+}=1$, 3, 5, 7 and 9 at.%, respectively. By using the above equation, we estimated the difference in electronegativity $\left(\chi\left(O^{2-}\right)-\chi\left(Eu^{3+}\right)\right)$, and the obtained values are shown in Table 1. Fig. 7 (a) shows the difference in electronegativity $\left(\chi\left(O^{2-}\right)-\chi\left(Eu^{3+}\right)\right)$ with different Eu^{3+} ion concentrations. The increase in energy for electron transfer in O^{2-} to Eu^{3+} clearly suggests a decrease in covalency and an increase in ionicity between O^{2-} and Eu^{3+}. The obtained results support the possible energy transfer between borate groups in the host to dopant Eu^{3+} ions. Several intense and sharp lines beyond 360 nm correspond to the direct excitation of the europium ground state into higher excited states of the europium *f*-electrons. The lines are ascribed to $^7F_0\rightarrow{}^5D_4$ (~362 nm), $^7F_0\rightarrow{}^5L_7$ (~376 nm and 382 nm), $^7F_0\rightarrow{}^5L_6$ (~394 nm and 400 nm), $^7F_0\rightarrow{}^5D_3$ (~414 nm), $^7F_0\rightarrow{}^5D_2$ (~465 nm) and $^7F_0\rightarrow{}^5D_1$ (~525 nm and 537 nm) transitions [30], which is found to be agree well with the DRS results. Moreover, it is observed that the Eu^{3+} ion does not have any absorption peak at ~355 nm. Literature overviews on the intensity of CTB compared with *f-f* transitions of Eu^{3+} ions have previously been published [27,31]. For instance, *Tian* and *co-workers* [27] reported that the intra configurational *f-f* transition of Eu^{3+} ions in $Y_2(MoO_4)_3:Eu^{3+}$ red phosphors are much more intense than that of the CTB of Eu - O. *Zhang et al.*,[31] prepared Eu^{3+}-, Tb^{3+}- or Tm^{3+}-activated $LaBGeO_5$ phosphors that had the CTB intensity values greater than that of the *4f-4f* transition of the Eu^{3+} ions. In our present work, the *f-f* transitions of the $NaSrB_5O_9:Eu^{3+}$ phosphor are greater than that of the CTB of Eu - O. Among several absorption bands, the dominant intense excitation peak at around 394 nm that corresponds to the $^7F_0\rightarrow{}^5L_6$ transition is used to study the emission spectra for all samples, which makes it very attractive for various applications, such as the red component of tricolor luminescence materials and white-lighting devices utilizing GaN-based excitations in near-UV light.

The emission spectra of the $NaSrB_5O_9:Eu^{3+}$ ($Eu^{3+}=0$, 1, 3, 5, 7 and 9 at.%) phosphors obtained by direct excitation of Eu^{3+} at 394 nm are displayed in Fig. 8. It can be seen that the emission spectra of the Eu^{3+}-doped $NaSrB_5O_9$ phosphor is composed of intense and sharp lines ranging from 560-720 nm, which are related to transition from the excited $^5D_0$ level to ^7F_J (J=0-4) levels; this is in contrast to the emission spectra of the pristine $NaSrB_5O_9$, which has an absence of emission lines (shown in the figure as a straight line) [32]. No significant shift in peak position is observed for the various Eu^{3+} ion concentrations. The characteristic peaks corresponding to Eu^{3+} *f-f* emission transitions at about 578 nm ($^5D_0\rightarrow{}^7F_0$), 592 and 602 nm ($^5D_0\rightarrow{}^7F_1$), 616 and 628 nm ($^5D_0\rightarrow{}^7F_2$), 655 nm ($^5D_0\rightarrow{}^7F_3$) and 695 and 703 nm ($^5D_0\rightarrow{}^7F_4$) are indicated in the figure. The crystal field splitting of both the magnetic dipole (MD) ($^5D_0\rightarrow{}^7F_1$) transition and electric dipole (ED) ($^5D_0\rightarrow{}^7F_2$) transition into two main lines each are also seen in the figure at 592, 602 nm and 616, 628 nm, respectively. The emission intensities for all the samples increased with the addition of active Eu^{3+}, which results in the enhancement of the red-emission of $NaSrB_5O_9:Eu^{3+}$ phosphors. In general, in the emission spectra of Eu^{3+}-doped phosphors, the main emissions are composed of two transitions: a typical MD $^5D_0\rightarrow{}^7F_1$ transition (orange) and a typical ED $^5D_0\rightarrow{}^7F_2$ transition (red). According to the electronic transition selection rules, the ED allowed transition can be dominant when Eu^{3+} occupies the lattice site of a non-centrosymmetric environment in the host matrix, while the MD transition does not depend on the local environment. From the XRD results, the $P2_1/c$ space group reveals that the prepared powders were crystallized in a non-centrosymmetric structure. For this reason, the intensity of $^5D_0\rightarrow{}^7F_2$ (ED transition) was found to be much stronger than that of $^5D_0\rightarrow{}^7F_1$ (MD transition). The $^5D_0\rightarrow{}^7F_2$ transition has a maximum emission intensity at ~616 nm. The emission spectrum of pristine $NaSrB_5O_9$ was recorded with an excitation peak at 282 nm and it is shown in Fig. 7 (b). The spectrum shows a broad UV emission band that peaks at ~362 nm, which may be due to the presence of intrinsic defect levels in the lattice during its synthesis [33]. The authors believed that the host emission is most reasonably assigned to the recombination of self-trapped excitons (STEs) that may be associated with band gap excitons or a molecular transition within the BO_3^{3-} group [34]. When Eu^{3+} ions are introduced to the $NaSrB_5O_9$ host matrix, an efficient energy transfer from host excitation to Eu^{3+} ions is expected. No other significant peaks were identified from 320–520 nm. To further confirm the energy transfer from host to Eu^{3+} ions, a 5 at.% Eu^{3+} ion-doped sample was excited with a 355 nm Nd-YAG laser and the emission spectrum is shown in Fig. 7 (c). The spectrum has both electric and magnetic transitions peaks. However, the emission intensity levels of these peaks are very small compared to direct Eu^{3+} ion excitation (i.e. weak energy transfer). Recently, *Parchur et al.* reported the Eu^{3+} emission (YPO_4:Eu) with an excitation wavelength below 350 nm and confirmed the energy transfer from intermediate/defect states

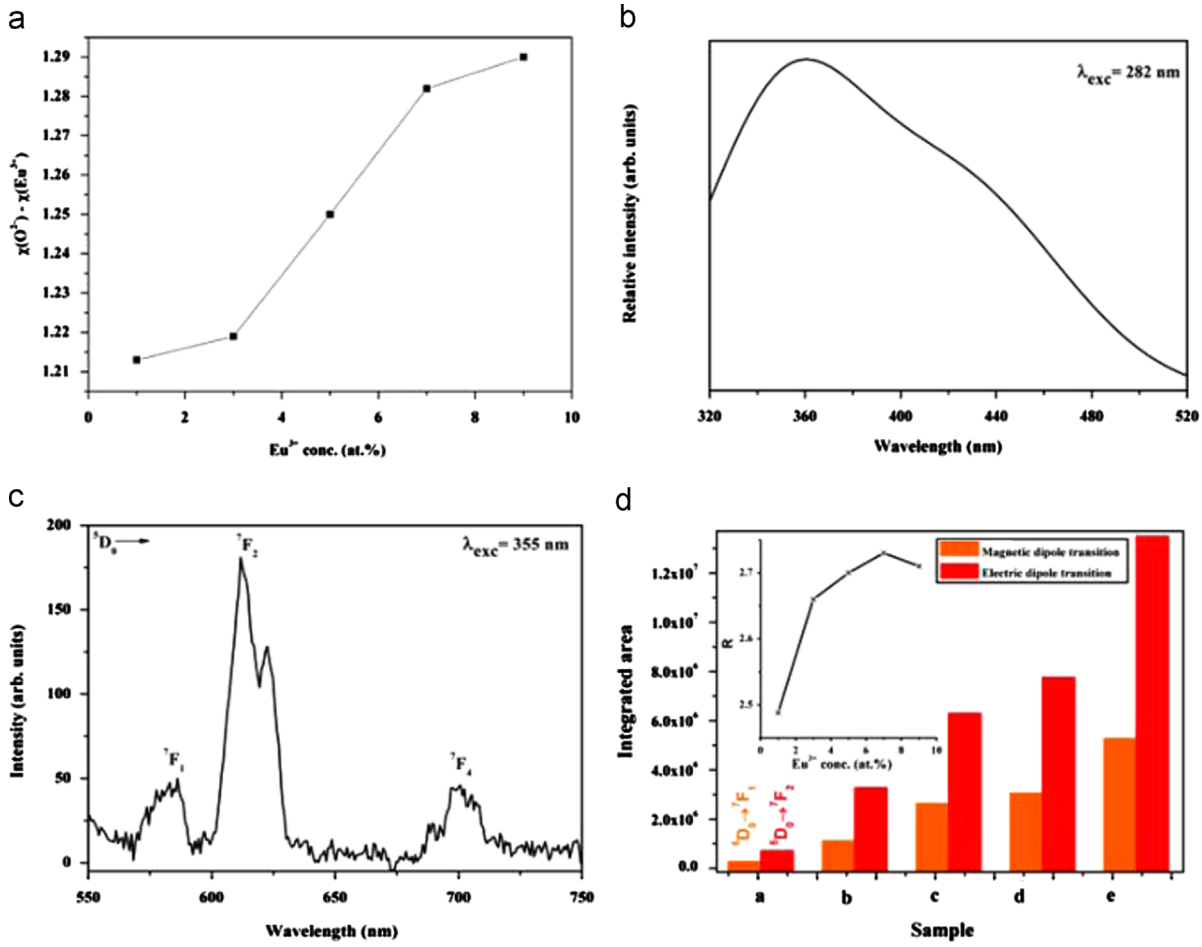

Fig. 7. (a) The difference in electronegativity $\left(\chi\left(O^{2-}\right)-\chi(Eu^{3+})\right)$ with various Eu^{3+} ion concentrations, (b) Emission spectrum (excited with 282 nm) of pristine $NaSrB_5O_9$, (c) Luminescence spectrum of $NaSrB_5O_9:Eu^{3+}$ (Eu^{3+}=5 at.%) phosphor excited with 355 nm Nd-YAG laser and (d) Integrated area of orange and red emission intensity distribution for $NaSr_{1-x}B_5O_9:Eu_x^{3+}$ (x=a – e=1- 9 at.%) phosphor. Inset shows the asymmetric ratios with various Eu^{3+} ion concentrations.

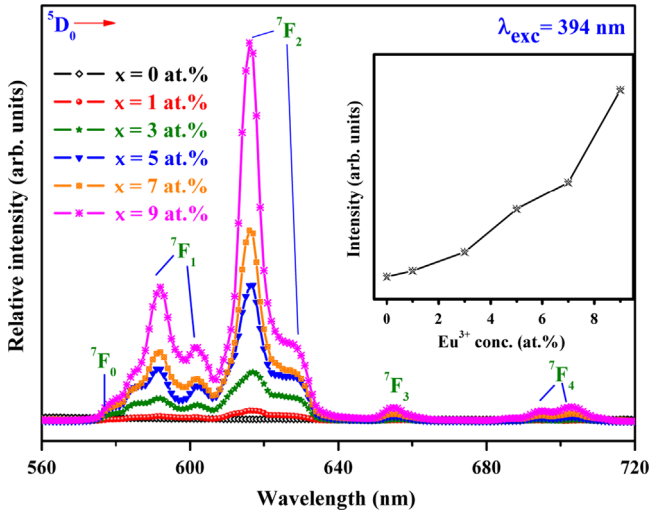

Fig. 8. Emission spectra of $NaSr_{1-x}B_5O_9:Eu_x^{3+}$ (x=0 – 9 at.%) phosphors. Inset shows the variation of PL intensity associated with different Eu^{3+} ion concentrations.

in the host to Eu^{3+} ions [35]. Hence, the obtained results indicated the weak energy transfer from host to Eu^{3+} ions. In addition, the environment of Eu^{3+} is determined by the asymmetric ratio (R), which is defined as the ratio of integrated emission intensities of ED to MD transitions [36],

$$R=\frac{\int {}^5D_0\rightarrow {}^7F_2}{\int {}^5D_0\rightarrow {}^7F_1}$$

The integrated intensities of MD and ED transitions for $NaSrB_5O_9:Eu^{3+}$ (Eu^{3+}=1, 3, 5, 7 and 9 at.%) are shown in Fig. 7 (d). The calculated asymmetric values with different Eu^{3+} ion concentrations are shown in the inset of Fig. 7 (d) and also presented in Table 1. The R values slightly increase as the Eu^{3+} ion concentration increases up to 7 at.% and then the R values began to decrease. The maximum R value was ~2.73 for this system. To further optimize the Eu^{3+} content in the host matrix, we carried out the experiment by varying the dopant concentration from 1 to 9 at.% with intervals of 2 at.%. Unfortunately, we could not find any quenching up to 9 at.%. Therefore, the solubility of Eu^{3+} ions in $NaSrB_5O_9$ may be 9 at.%.

3.8. CIE and color purity

The lighting specifications refers to color in terms of the 1931 CIE chromatic coordinates which recognizes that the human visual system uses three primary colors: red, green and blue. In general, the color of any light source can be represented on the (x, y) coordinates in this color space. The x and y values of the CIE chromaticity coordinates for the $NaSrB_5O_9:Eu^{3+}$ phosphors with different dopant contents were calculated using a CIE calculate software. Fig. 9 shows the CIE chromaticity diagram of the

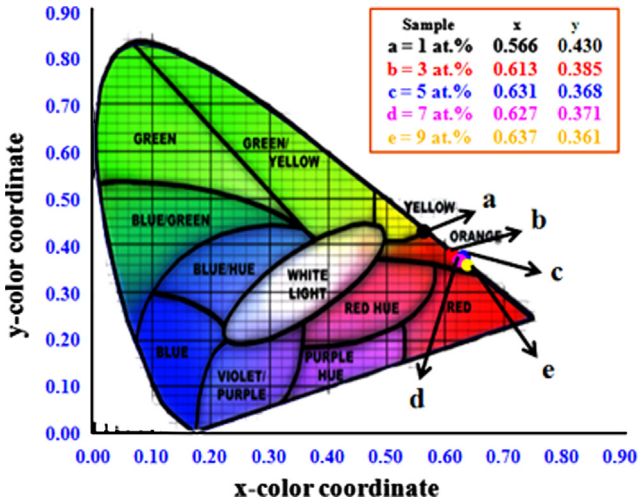

Fig. 9. CIE chromaticity coordinates of $NaSr_{1-x}B_5O_9:Eu_x^{3+}$ (x = a – e = 1 – 9 at.%) phosphors.

$NaSrB_5O_9:Eu^{3+}$ (Eu^{3+} = 1, 3, 5, 7 and 9 at.%) phosphor. The obtained values are located in the orange-red region, which is suitable for red components in LEDs. The color purity of the $NaSrB_5O_9:Eu^{3+}$ phosphor was compared to the standard chromaticity coordinates (0.33, 0.33). It is well known that the color purity or color saturation of a particular dominant color in a source is the ratio of the distance in the chromaticity diagram between the emission color coordinates and the coordinates of equal energy point to the distance between the equal energy point and the dominant wavelength point [37]. Hence, the color purity can be described by,

$$Color\ purity = \frac{\sqrt{(x-x_i)^2+(y-y_i)^2}}{\sqrt{(x_d-x_i)^2+(y_d-y_i)^2}} \times 100\%$$

where (x, y) and (x_i, y_i) are the color coordinates of the emission light and the CIE white illuminate (0.33, 0.33), respectively, and (x_d, y_d) are the chromaticity coordinates of the dominant wavelength points. The calculated color purity of the red $NaSrB_5O_9:Eu^{3+}$ phosphors are listed in Table 1. From the table, it is concluded that the $NaSrB_5O_9:Eu^{3+}$ samples have good color purity values and these values are comparable with previous reports [38,39].

4. Conclusions

In summary, we have prepared a new red-emitting $NaSrB_5O_9:Eu^{3+}$ (Eu^{3+} = 0, 1, 3, 5, 7 and 9 at.%) phosphor with the traditional one-step SSR method. The systematic structural analyses revealed that the prepared borates are formed with tetrahedron (BO_4) and trigonal (BO_3) borate groups in the $NaSrB_5O_9:Eu^{3+}$ phosphor. It is seen from the FE-SEM image that the phosphor is formed by nearly rod-like morphologies, which are several micrometers dimension. With the help of DRS analysis, the efficient energy transfer between borate groups to Eu^{3+} ions were discussed. The excitation spectrum of host matrix itself showed a broad absorption band peak at ~282 nm, indicating the energy transfer between B to O atoms in the $NaSrB_5O_9$. And this band shifted towards a lower wavelength region (i.e. higher energy) when the dopant Eu^{3+} ions were introduced into the $NaSrB_5O_9$ host lattices, strongly suggesting the possible energy transfer from borate groups to Eu^{3+} ions. Under the excitation of near-UV light (394 nm), PL spectra showed the characteristic sharp lines of the intra *4f-4f* transition of Eu^{3+}, ascribed to the $^5D_0 \rightarrow {}^7F_{0\text{-}4}$ transitions. Moreover, the estimated CIE chromaticity coordinates are in the orange-red region with high color purities around 99.7%. The above results demonstrated that $NaSrB_5O_9:Eu^{3+}$ phosphor might be a promising red-emitting phosphor for near-UV white LED applications.

Acknowledgement

The authors are sincerely thankful to the DRS facility and Dr. S. Kaleemulla, Assistant Professor in Physics, Materials Physics Division, School of Advanced Sciences, VIT University, Vellore. The authors also acknowledge the Sophisticated Analytical Instrumentation Facility (SAIF), IIT, Chennai for letting us utilize their instrumental facilities.

References

[1] Y.N. Xue, F. Xiao, Q.Y. Zhang, Spectrochim. Acta A 78 (2011) 1445–1448.
[2] G.R. Dillip, S.J. Dhoble, L. Manoj, C.M. Reddy, B.D.P. Raju, J. Lumin. 132 (2012) 3072–3076.
[3] C.R. Ronda, T. Justel, H. Nikol, J. Alloys Compd. 275–277 (1998) 669–676.
[4] V.R. Bandi, B.K. Grandhe, H.J. Woo, K. Jang, D.S. Shin, S.S. Yi, J.H. Jeong, J. Alloys Compd. 538 (2012) 85–90.
[5] S. Ye, F. Xiao, Y.X. Pan, Y.Y. Ma, Q.Y. Zhang, Mater. Sci. Eng. R 71 (2010) 1–34.
[6] M. Zhang, S. Pan, J. Han, Z. Zhou, J. Solid State Chem. 184 (2011) 825–829.
[7] M. Shang, G. Li, X. Kang, D. Yang, D. Geng, J. Lin, Appl. Mater. Inter 3 (2011) 2738–2746.
[8] F. Wang, H. Song, G. Pan, L. Fan, B. Dong, L. Liu, X. Bai, R. Qin, X. Ren, Z. Zheng, S. Lu, J. Lumin. 128 (2008) 2013–2018.
[9] J. Liu, X.D. Wang, Z.C. Wu, S.P. Kuang, Spectrochim. Acta A 79 (2011) 1520–1523.
[10] W. Park, R.Y. Lee, C.J. Summers, Y.R. Do, H.G Yang, Mater. Sci. Eng B78 (2000) 28–31.
[11] O.A. Lebbou, C. Goutaudier, S. Kubota, C. Dujardin, M. Th., C. Adad, C. Pedrini, P. Florian, D. Massiot, Opt. Mater. 16 (2001) 77–86.
[12] C.H. Huang, T.M. Chen, J. Phys. Chem. C 115 (2011) 2349–2355.
[13] L.S. Zhao, J. Liu, Z.C. Wu, S.P. Kuang, Spectrochim. Acta A 87 (2012) 228–231.
[14] J.D. Ghys, R. Mauricot, B. Caillier, P. Guillot, T. Beaudette, G. Jia, Peter A. Tanner, B.M. Cheng, J. Phys. Chem. C 114 (2010) 6681–6689.
[15] W.R. Liu, C.H. Huang, C.P. Wu, Y.C. Chiu, Y.T. Yeha, T.M. Chen, J. Mater. Chem. 21 (2011) 6869–6874.
[16] Z. Xia, J. Zhuang, L. Liao, Inorg. Chem. 51 (2012) 7202–7209.
[17] L. Wu, Y. Zhang, X.L. Chen, Y.F. Kong, T.Q. Sun, J.J. Xu, Y.P. Xu, J. Solid State Chem. 180 (2007) 1470–1475.
[18] A. Szczeszak, T. Grzyb, S. Lis, Rafal J. Wiglusz, Dalton Trans. 41 (2012) 5824–5831.
[19] G.R. Dillip, B.D.P. Raju, J. Alloys Compd. 540 (2012) 67–74.
[20] A. Pitscheider, R. Kaindl, O. Oeckler, H. Huppertz, J. Solid State Chem. 184 (2011) 149–153.
[21] Z.W. Jiao, F. Zhang, Q.F. Yan, D.Z. Shen, G.Q. Shen, J. Solid State Chem. 182 (2009) 3063–3066.
[22] K.N. Shinde, S.J. Dhoble, A. Kumar, J. Rare Earths 29 (2011) 527–535.
[23] C. Zhang, J. Shi, X. Yang, L. Lu, X. Wang, J. Rare Earths 28 (2010) 513–518.
[24] J. Sun, J. Lai, J. Sun, H. Du, J. Rare Earths 29 (2011) 321–325.
[25] H. Yang, J. Shi, M. Gong, H. Liang, J. Rare Earths 28 (2010) 519–522.
[26] Y.H. Sun, Y.X. Fu, J. Lumin. 132 (2012) 550–557.
[27] Y. Tian, X. Qi, X. Wu, R. Hu, B. Chen, J. Phys. Chem. C 113 (2009) 10767–10772.
[28] C.K. Jorgensen, Modern Aspects of Ligand Field Theory, Amsterdam, North Holland, 1971.
[29] A.K. Parchur, R.S. Ningthoujam, RSC Adv. 2 (2012) 10859–10868.
[30] F. Xiao, Y.N. Xue, Q.Y. Zhang, Spectrochim. Acta A 74 (2009) 498–501.
[31] S. Zhang, G. Wu, C. Duan, J. Wang, J. Rare Earths 29 (2011) 737–740.
[32] C. Lorbeer, J. Cybinska, A.V. Mudring, Cryst. Growth Des. 11 (2011) 1040–1048.
[33] G. Anoop, K. Muni Krishna, M.K. Jayaraj, J. Electrochem. Soc. 155 (2008) J7–J10.
[34] D.Y. Wang, T.M. Chen, B.M. Cheng, Inorg. Chem. 51 (2012) 2961–2965.
[35] A.K. Parchur, A.I. Prasad, S.B. Rai, R. Tewari, R.K. Sahu, G.S. Okram, R.A. Singh, R.S. Ningthoujam, AIP Adv. 2 (2012). (032119-15).
[36] B. Antic, J. Rogan, A. Kremenovic, A.S. Nikolic, M.V. Vasic, D.K. Bozanic, G.F. Goya, Ph. Colomban, Nanotechnol. 21 (2010). (245702-7).
[37] J.S. Kumar, K. Pavani, A.M. Babu, N.K. Giri, S.B. Rai, L.R. Moorthy, J. Lumin. 130 (2010) 1916–1923.
[38] Z. Loua, J. Hao, Thin Solid Films 450 (2004) 334–340.
[39] M. Ferhi, K.H. Naifer, M. Ferid, J. Rare Earths 27 (2009) 182–186.